Food Chemistry 319 (2020) 126570

Contents lists available at ScienceDirect

Food Chemistry

journal homepage: www.elsevier.com/locate/foodchem

Preparation of a novel emulsifier by self-assembling of proanthocyanidins from Chinese bayberry (*Myrica rubra* Sieb. et Zucc.) leaves with gelatin

Shiguo Chen*, Xuemin Shen, Wenyang Tao, Guizhu Mao, Wenyan Wu, Shengyi Zhou, Xingqian Ye, Haibo Pan*

Zhejiang University, College of Biosystems Engineering and Food Science, Zhejiang Key Laboratory for Agro-Food Processing, Fuli Institute of Food Science, Zhejiang R & D Center for Food Technology and Equipment, Hangzhou 310058, PR China

ARTICLE INFO

Keywords:
Proanthocyanidins
Gelatin
Colloidal complexes
Novel emulsifier
Physicochemical stability

ABSTRACT

A physicochemically stable emulsion was developed by using a novel emulsifier, which was self-assembled colloidal complex of gelatin (GLT) and proanthocyanidins from Chinese bayberry (*Myrica rubra* Sieb et Zucc.) leaves (BLPs), with epigallocatechin-3-O-gallate (EGCG) as structure units. The GLT–BLP colloidal complexes were spherically shaped by transmission electron microscope (TEM). The data of Fourier transform infrared spectrum (FTIR), circular dichroism (CD), isothermal titration calorimetry (ITC) revealed that the main binding force between GLT and BLPs of the colloidal complexes was hydrogen bond. The incorporation of BLPs to GLT provided GLT with stronger affinity at oil-water interface and thus enhanced the physical stability of GLT-stabilizing emulsion. In addition, the emulsions stabilized by the colloidal complexes showed higher oxidation stability than that stabilized by free GLT only. The novel emulsifier developed in this study have potential applications as functional emulsifiers in food-grade emulsions with high anti-oxidation activity.

1. Introduction

Proanthocyanidins (PAs), also called condensed tannins, are a class of secondary metabolites of plants, characterized by an oligomeric or polymeric structure based on flavan-3-ol units (Ou & Gu, 2014). They have diverse biological properties, including antioxidant, antibacterial, and antiviral properties (Smeriglio, Barreca, Bellocco, & Trombetta, 2017). Proanthocyanidins from Chinese bayberry (*Myrica rubra* Sieb. et Zucc.) leaves (BLPs) have epigallocatechin-3-O-gallate (EGCG) as their terminal unit and extension units (Fu et al., 2014). Compared with other PAs (Hammerstone et al., 2004; Naczk & Shahidi, 2006) from cranberry or grape seeds, with catechin, epicatechin, and galloatechin as terminal and extension units, BLPs show stronger antioxidant activity due to containing more active phenolic hydroxyl. But at the same time, BLPs have high water solubility, which inhibits their penetration into food oily system and thus decreases a certain degree of antioxidant activity. Thus it is crucial to find a way to enhance the solubility of BLPs in oily systems.

Gelatin (GLT) is one of the most traditional multifunctional food ingredients used as a stabilizer, thickener, and texturizer. It's a biodegradable protein obtained by acid- or base-catalyzed hydrolysis of collagen. Several previous studies attempted to use GLT to prepare physically stable emulsions, but hardly met the expected results (Surh, Decker, & McClements, 2006; Zarai, Balti, Sila, Ali, & Gargouri, 2016). GLT has some emulsifying ability, but it is not sufficient to form physically stable oil-in-water emulsions, which limits the use of GLT as a protein emulsifier (Lobo, 2002). What's more, protein-based emulsions are prone to chemical destabilization mostly through oxidative reactions that degrade protein and polyunsaturated lipids during processing and storage (Berton & Schroen, 2015).

The polymer complexation can provide an effective way to improve the antioxidant activity of protein and the surface activity of polyphenols. GLT molecules have unique triple helix structures due to their repeating sequences of alanine, proline, and glycine, which determine the high stability of GLT colloidal complexes. In addition, GLT, rich in proline, has extended random coil conformation which provides more interaction sites for self-assembly of colloidal complexes. Self-assembly of GLT with tannin acids (Huang, Li, Qiu, Teng, & Wang, 2017), ellagitannins (Li & Gu, 2011), and catechins (Chen et al., 2010) has been used to prepare GLT colloidal complexes. The affinity of polyphenols determines the characteristics of GLT colloidal complexes. As we know, BLPs contain oligomeric and polymeric forms. The oligomeric forms receive attention in view of their antioxidant activity while the polymeric forms have stronger affinity to proteins (Zou, Li, Percival,

* Corresponding authors at: College of Biosystems Engineering and Food Science, Zhejiang University, Yuhangtang Road 866#, Hangzhou 310058, PR China.
E-mail addresses: chenshiguo210@163.com (S. Chen), apanhaibo@126.com (H. Pan).

https://doi.org/10.1016/j.foodchem.2020.126570
Received 6 September 2019; Received in revised form 29 February 2020; Accepted 4 March 2020
Available online 05 March 2020

Bonard, & Gu, 2012). Therefore, GLT could form highly stable colloidal complexes with BLPs due to this high affinity. In addition, the molecular backbone of BLPs consists of a chain of aromatic rings. BLPs molecules tend to form a network between GLT colloidal complexes due to intermolecular aromatic interactions (Waters, 2013), which could enhance the stability of emulsions.

The objective of this study was to elucidate the potential of GLT–BLP colloidal complexes as effective food-grade emulsion stabilizers. The characteristics of GLT–BLP colloidal complexes, including their physical properties, morphologies, and interaction forces, were studied to provide a better understanding of the interaction between them. Furthermore, the physicochemical stabilities of emulsions stabilized by the colloidal complexes were evaluated.

2. Materials and methods

2.1. Materials

GLT (from porcine skin, type B), soybean oil, Nile red, and Nile blue were purchased from Aladdin Bio-Chem Technology Co., Ltd (Shanghai, China). BLPs were extracted from Chinese bayberry leaves (from Zhejiang Cixi, China) and purified according to our previous studies (Fu et al., 2014; Zhang et al., 2016). The composition of BLPs was shown in Table 1. All other chemicals used were of analytical grade.

2.2. Preparation of GLT–BLP colloidal complexes

GLT–BLP colloidal complexes were prepared according to the method described in a previous paper (Su et al., 2015). Both GLT and BLPs stock solutions at the concentration of 1.2 wt% were prepared by dissolving GLT and BLPs in distilled water. GLT–BLP colloidal complexes were prepared using a simple, self-assembly method under magnetic stirring (200 rpm) at room temperature (25 °C) for 30 min. Colloidal complexes were fabricated by adding BLPs solution to GLT solution with mass ratios of 0:10, 1:9, 2:8, 3:7, 4:6, and 5:5, respectively. The final colloidal complex solutions contained 0.1, 0.2, 0.3, 0.4, and 0.6 wt% GLT.

2.3. Physical properties and morphology of colloidal complexes

The light transmittance of the GLT–BLP solutions was measured at ambient temperature using a UV–vis spectrophotometer (UV-2550, Shimazu, Japan) at a wavelength of 500 nm. The mean particle sizes and ζ-potential values of the colloidal complexes were measured with a Zetasizer (Nano ZS90, Malvern Instruments Ltd, UK) at 25 °C. Samples were first diluted 100 times with distilled water and stirred to induce the breakup of large aggregates.

The morphology of the colloidal complexes was examined by transmission electron microscopy (TEM). The sample was prepared by placing a drop of the test suspension onto a 400 mesh, carbon–coated copper grid. About 2 min after deposition, the grid was tapped with filter paper to remove surface water, followed by air-drying. Then, the dried samples were observed by TEM.

Table 1
The composition of BLPs.

Compound	Content (%)
Epigallocatechin	0.81
Epigallocatechin gallate	2.73
Proanthocyanidin (HPLC area)	93.46
Protein	1.76
Polysaccharide	1.31
Ash	0.13

2.4. Fourier transform infrared (FTIR) spectroscopy

The chemical structures of BLPs, GLT, and GLT–BLP colloidal complexes were analyzed with Fourier transform infrared (FTIR) spectra. Specifically, 3 mg samples were ground together with 200 mg of KBr and analyzed by FTIR in the frequency range of 4000–400 cm^{-1}, with 32 scans and a 4 cm^{-1} resolution. FTIR spectra were taken on a Nicolet Avatar 370 instrument.

2.5. Circular dichroism (CD)

Circular dichroism (CD) spectrum was obtained on a Jasco 715 circular dichroism spectropolarimeter according to previous study (Su et al., 2015), which was scanned at a speed of 50 nm/min with a slit width of 1 nm. The spectra were recorded under a N_2 atmosphere in the far UV region (190–280 nm) to estimate the conformational change in GLT with the BLPs solution. The samples were analyzed at 25 °C in a 0.1 mm path length quartz cell. Different volumes (20, 40, 60, and 80 μL) of BLP (0.2 wt%) solution were added to an aqueous solution of GLT (0.03 wt%, 1 mL). After subtracting the reference spectrum (solvent peak), the data were normally plotted as mean–residue–weight ellipticity (deg cm^2 $dmol^{-1}$) versus wavelength in nanometers. Changes in the conformation of GLT upon addition of various amounts of BLP were recorded.

2.6. Isothermal titration calorimetry (ITC)

The thermodynamics of the binding of BLPs to GLT were assessed using a isothermal titration calorimeter (ITC) (Microcal UC, USA). The reference cell was filled with deionized water, while the sample cell was filled with GLT solution (2 μM). The injection syringe, filled with 800 μM of BLPs solution, was titrated into the sample cell as a sequence of 20 injections of 2 μL aliquots with 300 rpm stirring at 25 °C. Raw data were obtained as a plot of heat against the injection number. These raw data were then integrated to obtain a plot of the observed enthalpy change per mole of the injection ($\triangle H_{obs}$, kJ) against the molar ratio.

2.7. Interfacial adsorption kinetics

The interfacial force of protein and its colloidal complexes at the oil–water interface was measured by the pendant drop technique with an optical contact angle meter (OCA-20, Data-physics Instruments GmbH, Germany) at ambient temperature. All aqueous solutions were used with a GLT concentration of 0.4 wt%, and the cuvette, syringe, and needle were cleaned intensively prior to each measurement. The interfacial tension was monitored for 1 h while keeping a drop of solution in soybean oil. The interfacial force was calculated according to the fundamental Laplace equation.

2.8. Preparation of oil–in–water (O/W) emulsion and measurements of its particle size and ζ-potential

Coarse emulsions were prepared by homogenizing soybean oil with only GLT or with GLT–BLP colloidal complex solutions at different concentrations using an FSH-2A digital homogenizer (China) for 3 min under 12,000 rpm. The oil content was kept at 20 wt%. This coarse emulsion was then passed through a high-pressure homogenizer (NanoGenizer30K, Genizer, USA) 3 times at 50 Mpa. The mean droplet sizes and ζ-potentials of the final emulsions were measured with a Zetasizer (Nano ZS90, Malvern Instruments Ltd, UK), with a refractive index of 1.472 and 1.330 for the dispersed phase and the continuous phase, respectively. Samples were first diluted 100 times and stirred to induce the breakup of large aggregates. All experiments were performed three times.

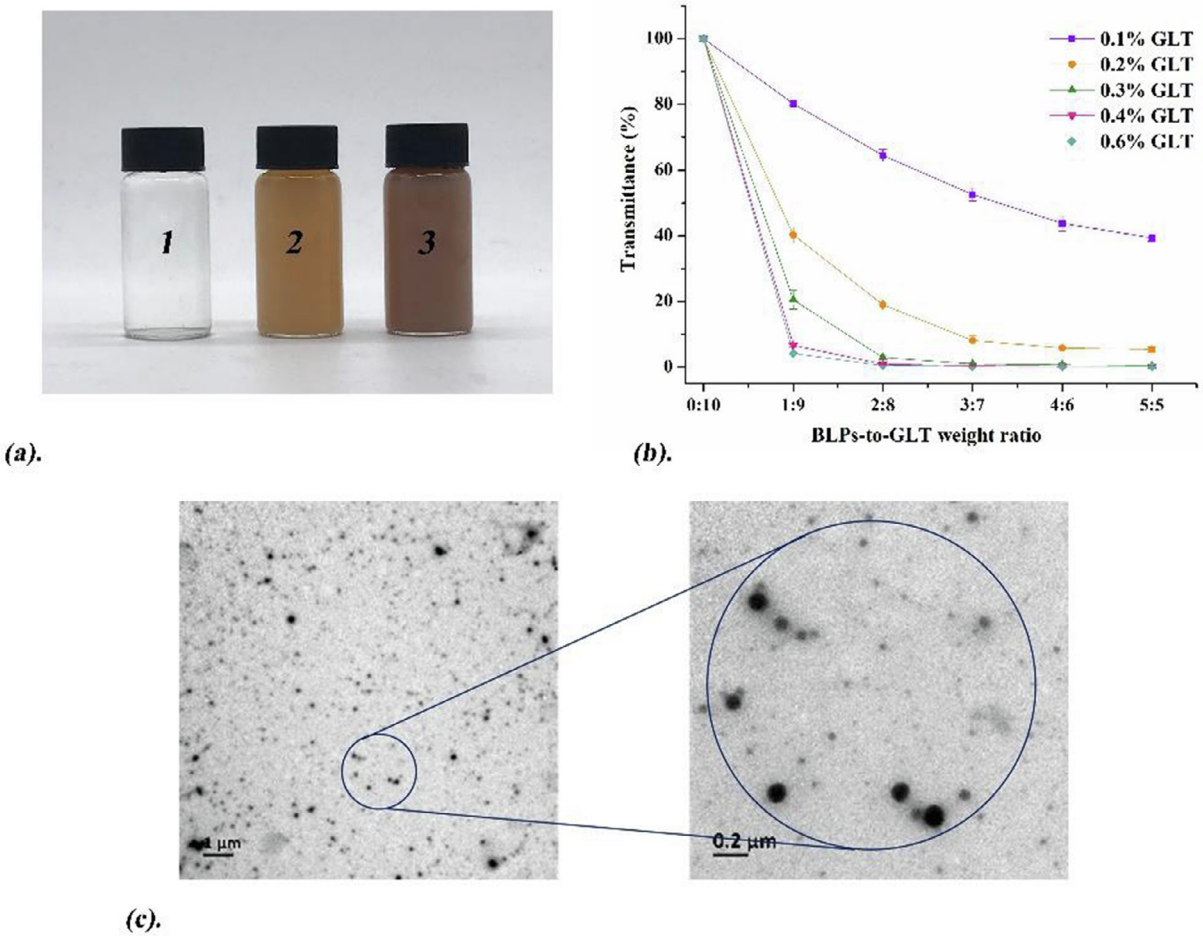

Fig. 1. Visual appearance of colloidal complexes (1 refers to 0.6% GLT, 2 refers to 0.6% GLT–0.15% BLPs, 3 refers to 0.6% GLT–0.6% BLPs) (a), transmittance of GLT–BLP colloidal complexes at various concentrations and mass ratios (b), and transmission electron microscope (TEM) images of GLT–BLP colloidal complexes (0.2% GLT–0.05% BLP) (c).

2.9. Confocal laser scanning microscopy (CLSM)

The confocal laser scanning microscopy (CLSM) (TCS SP8, Leica microsystems, Germany) was used to investigate the microstructure of the emulsion. An aliquot (1 mL) of the emulsion was dyed using 15 μL of Nile Red solution (0.1 wt%, in isopropyl alcohol) and 15 μL of Nile Blue A (0.1 wt%, in isopropyl alcohol). One drop of the dyed emulsion was placed on a concave slide, followed by covering it with a coverslip. The CLSM pictures were obtained by using a 488 nm (for Nile Red) and 633 nm (for Nile Blue A) laser to excite the samples.

2.10. Lipid oxidation in soybean oil emulsions

The soybean oil emulsions stabilized by only GLT and by GLT–BLP colloidal complexes were prepared according to the process mentioned above. Samples were maintained at 30 °C and were taken every two days for the determination of the peroxide value (PV) and the quantity of thiobarbituric acid-reactive substances (TBARS) over a 14-day storage period.

2.10.1. Peroxide value (PV)

Lipid hydroperoxide measurement of soybean oil emulsions was performed according to a previous study (Tong, Sasaki, McClements, & Decker, 2000), with slight modification. In brief, 0.3 mL of the emulsion were mixed with 1.5 mL of isooctane/isopropanol (3/1, v/v) and vortexed three times, and the organic phase was collected by centrifugation at 5000 rpm for 2 min. About 0.2 mL of the supernatant were added to 2.8 mL of methanol/1-butanol (2/1, v/v), followed by the addition of 15 μL of 3.94 M NH_4SCN solution and 15 μL of Fe^{2+} solution, which was produced by blending $FeSO_4$ and $BaCl_2$ to a final concentration of 0.144 and 0.132 M, respectively. The sample was thoroughly mixed and left at ambient temperature in the dark for 20 min. The absorbance was measured with a spectrophotometer (UV-2550, Shimadzu, Japan) at 510 nm. Lipid hydroperoxide, expressed as mmol hydroperoxide per kg oil, was quantified using the standard curve established by cumene hydroperoxide standard solutions.

2.10.2. Thiobarbituric acid-reactive substances (TBARS)

TBARS values were determined according to a previous study (Qiu, Zhao, Decker, & McClements, 2015), with slight modification. About 1 mL of the emulsion sample was mixed with 4 mL of thiobarbituric acid (TBA) reagent, which was prepared by dissolving 0.375 g of TBA (0.375%, w/v) and 15 g of trichloroacetic acid (TCA) (15%, w/v) in 100 mL of 0.25 M HCl. The obtained mixture was heated in a boiling water bath for 15 min and then immediately cooled to room temperature with tap water. The resultant mixtures were then centrifuged for 15 min at 6000 rpm. The absorbance was measured at 532 nm using a spectrophotometer (UV-2550, Shimadzu, Japan). TBARS concentrations were calculated from a standard curve of 1,1,3,3-tetramethoxypropane.

2.11. Statistical analysis

All measurements were carried out in triplicate trails, each with a

new batch of sample preparation, the statistical significance was analyzed using IBM SPSS 20.0 software. Data were subjected to analysis of variance (ANOVA), and the Duncan's Test was used for mean comparison. The level of significance was set at $p < 0.05$.

3. Results and discussion

3.1. Characteristics of colloidal complexes

3.1.1. Light transmittance and morphology

It is known that PAs can strongly bind to proteins, leading to the alteration of their physicochemical properties. The visual appearance, light transmittance (%T) values, and TEM images of colloidal complexes were obtained to study the physicochemical properties of GLT induced by BLPs addition. Aqueous solutions of both GLT and BLPs were clear and transparent. A mixture of them formed a turbid solution (Fig. 1a), which indicated that an interaction between GLT and BLPs occurred. The light transmittance results from the scattering and absorption of light by dispersed colloidal complexes, which is determined by the size and number of the colloidal complexes (Linke & Drusch, 2016). The light transmittance decreased with increasing BLPs concentration (Fig. 1b), which suggested that the size or number of GLT–BLP colloidal complexes increased with increasing BLPs concentration. To confirm the formation of GLT–BLP colloidal complexes, TEM was used to characterize their morphologies. As shown in Fig. 1c, GLT–BLP colloidal complexes were spheres with smooth surfaces, which were similar to colloidal complexes formed with GLT and PAs from grape seed (Su et al., 2015; Huang et al., 2017). The units of PAs, such as EGCG and catechin have also been reported to interact with GLT to form spherical colloidal complexes (Huang et al., 2018; Chen et al., 2010). As reported, the higher molecular weight of polyphenols, the stronger interaction between polyphenols and protein (Le Bourvellec & Renard, 2012). The molecular weight of BLPs was significantly higher than simple polyphenols, including EGCG and catechin, which suggested higher stability of GLT–BLP complexes than GLT–EGCG complexes and GLT–catechin complexes.

3.1.2. Particle size and ζ-potential

The influence of GLT and BLPs concentrations on the size and ζ-potential of the colloidal complexes was further investigated. The mean particle size, PDI and ζ-potential of GLT–BLP colloidal complexes prepared at various concentrations are shown in Fig. 2. Mean particle sizes of the colloidal complexes generally decreased as the weight ratios of BLP to GLT increased (Fig. 2a). Meanwhile, the sizes of the colloidal complexes increased as the concentration of GLT increased at the same GLT–to–BLP weight ratios. PDI of the size distribution ranged from 0.09 to 0.20, which inidicated the size distribution of the colloidal complexes was uniform. However, the addition of BLPs to the GLT solution at high concentrations led to coagulation of GLT-BLPs colloidal complexes (Zhou, Yan, Yin, Tang, & Yang, 2018; Zou et al., 2012). Thus, we chose GLT–to–BLP weight ratios of 4:1 and 8:1 for further preparation of emulsions.

The ζ-potentials of colloidal complexes are shown in Fig. 2c. The ζ-potentials of the colloidal complexes were negative and decreased as GLT-to-BLP weight ratios decreased. The pH values of both BLPs and GLT stock solution were 4.6 and 6.8 and the pH values of the GLT–BLP colloidal solutions ranged from 6.2 to 6.5, which indicated BLPs were the major factors that contributed to the negative ζ-potential (Huang et al., 2017). ζ-Potential plays an important role in the physical stabilities of disperse systems (Gohtani & Yoshii, 2018). High ζ-potential helps the complexes repel each other, which avoids aggregation and coalescence. The decreased negative ζ-potential should lead to enhanced stability of GLT-BLPs colloidal complexes, which would further influence the stability of emulsion stabilized by the colloidal complexes.

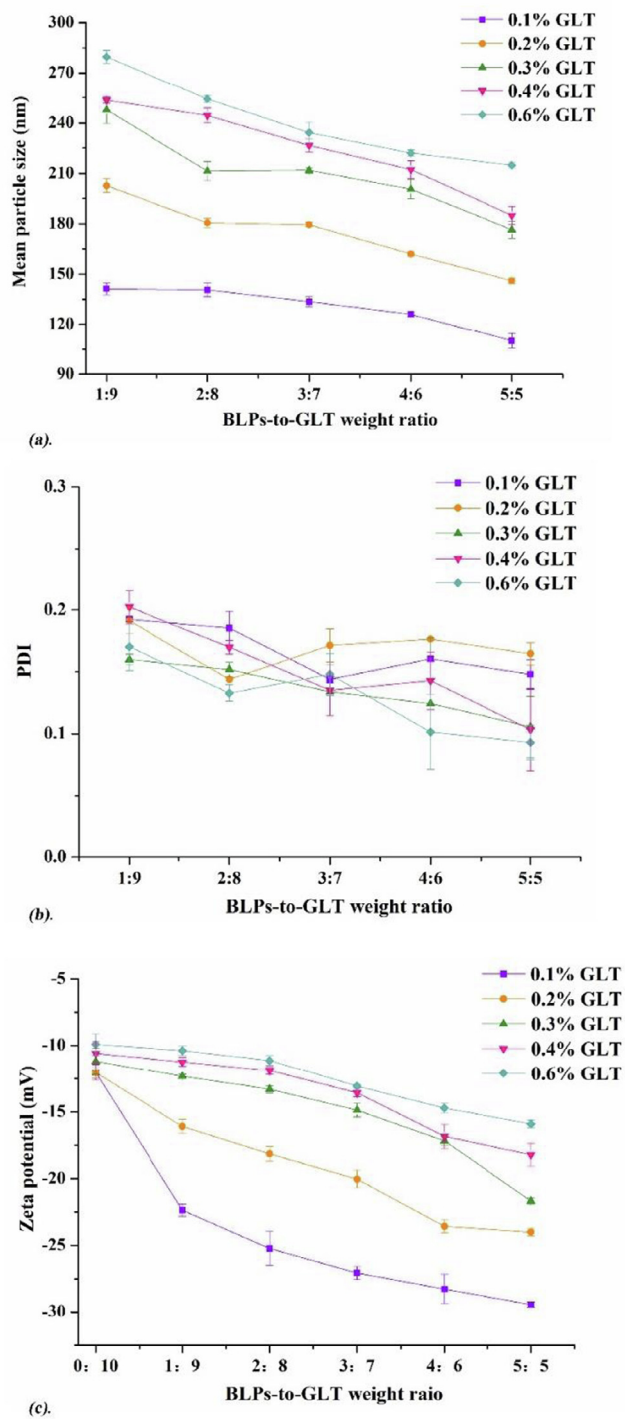

Fig. 2. The mean particle size (a), polydispersity index (PDI) (b) and ζ-potential (c) of GLT–BLP colloidal complexes prepared at various concentrations.

3.2. The binding characteristics of GLT and BLPs

The interactions between proteins and polyphenols are usually noncovalent and hydrophobic interactions and hydrogen bonding. To elucidate the binding characteristics of GLT and BLPs, FTIR, CD, and ITC analyses were carried out. Fig. 3a showed the FTIR spectra of GLT, BLPs and their interacted colloidal complexes at different weight ratio. The spectrum of GLT exhibited a broad peak in the region of 3700–3000 cm^{-1} related to the O—H and N—H stretching vibration, as well as a group of bands in the region of 3000–2800 cm^{-1} assigned to C—H stretching vibrations. The absorption peaks of GLT at about

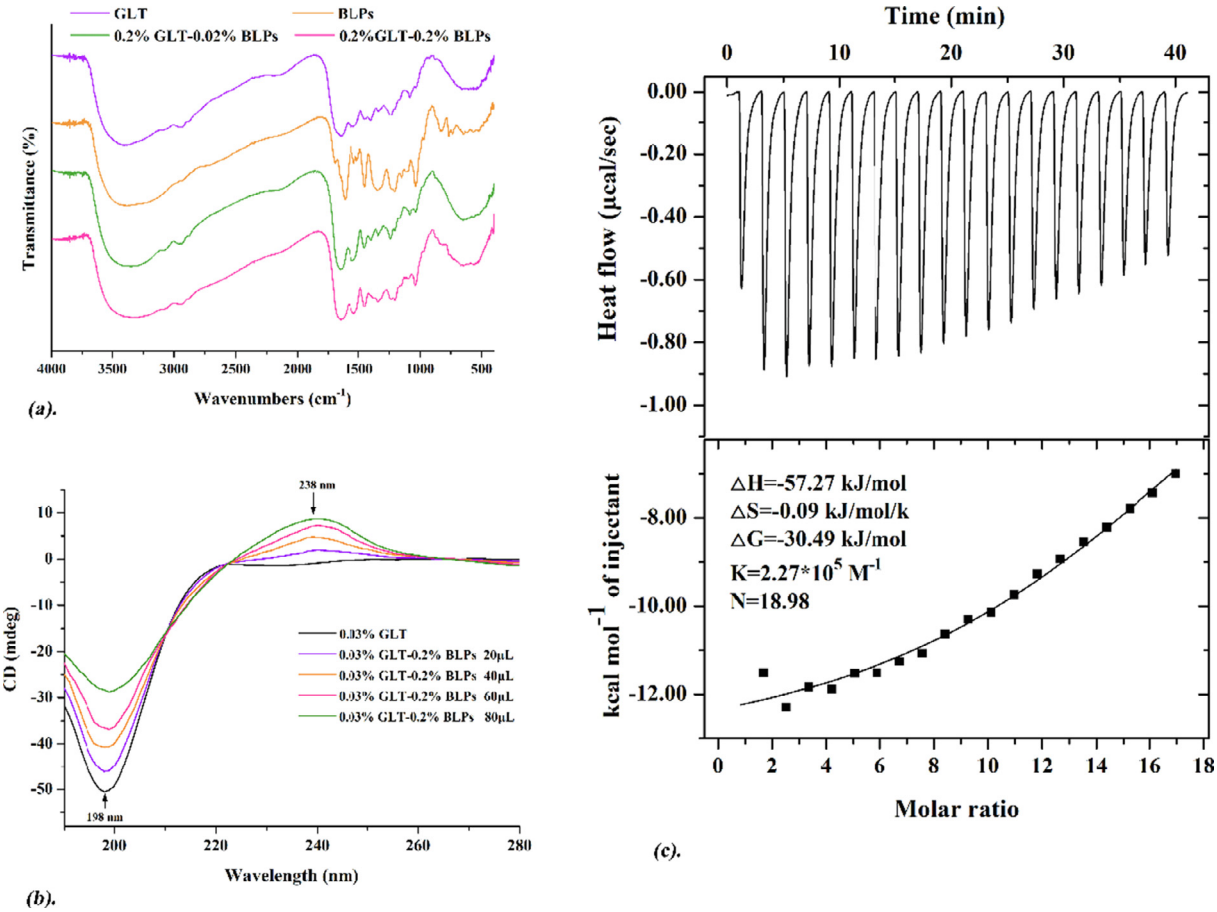

Fig. 3. Fourier transform infrared (FTIR) spectra of GLT, BLPs, and GLT–BLP colloidal complexes (a); Circular dichroism (CD) spectra of GLT binding with different amounts of BLPs (b); and Isothermal titration calorimetry (ITC) binding isotherms and heat flow against time for GLT with BLPs (c).

1653 cm^{-1}, 1540 cm^{-1}, and 1237 cm^{-1} were related to amide I, amide II, and amide III, respectively. The results is consistent with the report of gelatin from skins and bones (Muyonga, Cole, & Duodu, 2004). The chemical structure of BLPs can be characterized by the FTIR absorptions of catechins and epicatechin and their gallic acid esters (Ricci, Olejar, Parpinello, Kilmartin, & Versari, 2015). The broad bands observed at around 3385 cm^{-1} is attributed to the vibration of the O—H linkage of phenolic hydroxyl groups. BLPs demonstrates absorption bands at 1612, 1514, 1448, 1343, 1205, 1147, 1035, and 825–736 cm^{-1}, which are assigned to C═C stretch (aromatic ring), C—H stretch (alkanes), —C—O stretch (alcohols), C—O—C stretch (ether), and ═C—H out-of-plane bending (aromatic ring) (Liu, Li, Yang, Xiong, & Sun, 2017; Ricci et al., 2015). The FTIR spectra of GLT–BLP colloidal complexes was identical to that of only GLT, indicating that the interaction between GLT and BLPs was non-covalent bonding (Ferraro et al., 2015). The formation of GLT–BLP colloidal complexes led to several shifts in their bands. The O—H peak of the colloidal complexes shifted from 3385 cm^{-1} to 3316 cm^{-1} and the band became wider, which indicated that the interaction between GLT and BLPs was hydrogen bonding (Liu et al., 2017). The band shifts were also observed at amide I (from 1653 cm^{-1} to 1641 cm^{-1}) and amide II (from 1540 cm^{-1} to 1524 cm^{-1}).

The CD spectra of GLT and GLT–BLP colloidal complexes performed in the wavelength range of 190–280 nm could provide secondary structural information on their polypeptide backbones. Changes in the secondary structure of GLT, examined with the CD spectra, are shown in Fig. 3b. The interaction between GLT and BLPs led to a positive ellipticity around 238 nm, suggesting that GLT reassembled to form the triple helical-like structure (Su et al., 2015). Thus, interaction between GLT and BLPs induced the alteration of intramolecular hydrogen bonds, which formally defined the secondary structure of GLT.

A thermodynamic technique for identifying biomolecular interaction, ITC, was further used to determine the binding characteristics between GLT and BLPs. The binding isotherms were shown as a plot of heat flow against BLP–to–GLT molar ratio, and the data for the interactions were fitted to binding models to determine the thermodynamic parameters (Fig. 3c). An exothermic interaction ($\Delta H = -57.27$ kJ/mol) implied that binding between BLPs and GLT was strong. In addition, the relatively low enthalpy value indicated that hydrogen bonding played an essential role in the formation of colloidal complexes due to the —OH groups of the polyphenol molecules. The negative value of entropy ($\Delta S = -0.09$ kJ/mol) implied that the interaction was driven by enthalpy, resulting in decreased disorder, which was similar to the interaction between sunflower proteins and phenols (Karefyllakis, Altunkaya, Berton-Carabin, van der Goot, & Nikiforidis, 2017). The negative value of Gibbs free energy ($\Delta G = -30.49$ kJ/mol) indicated that the interaction between GLT and BLPs occurred spontaneously. The equilibrium binding constant (K) was calculated to be 2.27×10^5 M^{-1}, suggesting that the binding between BLPs and GLT was quite strong. The stoichiometry number ($N = 18.98$) suggested that BLPs were bound to GLT at multiple sites, which was consistent with the previous study of the interaction between tannins and GLT (Huang et al., 2017).

In summary, hydrogen bonding plays an essential role in the binding of GLT with BLPs to form colloidal complexes.

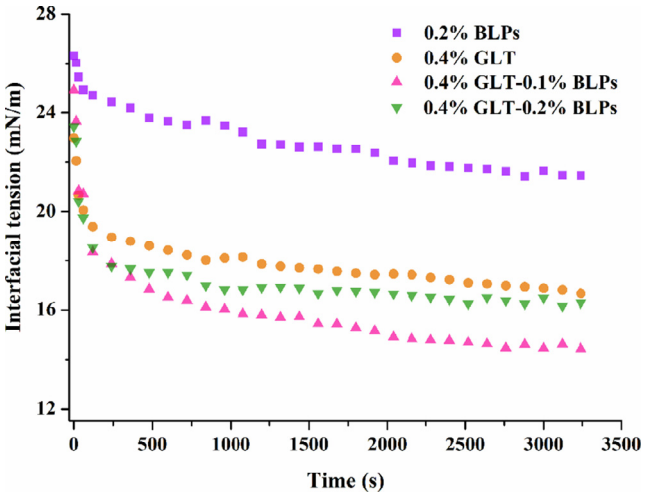

Fig. 4. Time evolution of interfacial tension affected by BLPs, GLT, and GLT–BLP colloidal complexes.

3.3. Interfacial behavior of the colloidal complexes

To test the potential of GLT–BLP colloidal complexes in stabilizing oil-in-water (O/W) emulsions, the interfacial tension of the droplet surface was determined. The absorption of the emulsifiers at the interface comprises two stages. First, the amphiphilic molecules approach and attach to the droplet surface, leading to a rapid decrease in the interfacial tension. Second, these molecules are rearranged and the interfacial tension decreases gradually to a balanced value (Rao, Kim, & Thomas, 2005). As shown in Fig. 4, the interfacial tension decreased rapidly upon adsorption of GLT–BLP colloidal complexes onto the interface, followed by a slow decrease. Obviously, the interfacial tension was decreased more by GLT–BLP colloidal complexes than by GLT or BLPs only, which was consistent with results reported previously (Qiu, Huang, Li, Ma, & Wang, 2018). However, the interfacial tension increased as BLP–to–GLT weight ratios increased, which was probably attributed to the reduced hydrophobic area of GLT, induced by the interaction of GLT with excess BLPs (Chung et al., 2014). Thus, the interfacial tension induced by colloidal complexes with high mass ratio of BLPs to GLT reduced less severely than that with low mass ratio of BLPs to GLT. However, the stability of colloidal complexes with high mass ratio of BLPs to GLT would be much higher than that with low mass ratio of BLPs to GLT. So, the mass ratio of BLPs to GLT is a pivotal factor that balances interfacial tension and stability of colloidal complexes.

3.4. Emulsion droplet size distribution, ζ-potential, and CLSM

The droplet size distribution and ζ-potential of emulsions stabilized by GLT and GLT–BLP colloidal complexes were measured to assess their emulsifying ability. As shown in Fig. 5a and Fig. 5b, the emulsions stabilized by GLT–BLP colloidal complexes exhibited a narrower size distribution and smaller size than that of GLT only. As shown in Fig. 5b, the negative ζ-potential of the droplets decreased with the increase in BLP–to–GLT mass ratios. Thus, the emulsions stabilized by GLT–BLP colloidal complexes showed higher stabilities compared with the emulsions stabilized by GLT only (Fig. 5c). It's known that droplet size and ζ-potential play important role in emulsion stability (Goodarzi & Zendehboudi, 2019). The reduced size and negative ζ-potential induced by the formation of GLT–BLP colloidal complexes were the major factors that enhanced the stability of emulsion stabilized by the colloidal complexes. Besides, BLP molecules have a tendency to form network due to hydrogen bond and aromatic interaction (Scott & Fernández, 2017). The network among the colloidal complexes was able to enhance the stability of shell on the surface of lipid droplets and further improve the stability of emulsion stabilized by the colloidal complexes. The network formation capacity of PAs was also used to improve the mechanical properties and thermal stability of chitosan film (Kim, Nimni, Yang, & Han, 2005; Bi et al., 2019).

Emulsion microstructures were characterized with CLSM. Lipid droplets and GLT–BLP colloidal complexes were dyed with Nile Red (green) and Nile Blue A (red), respectively. As shown in Fig. 5d, the colloidal complex layer (red) adsorbed on the outer layer of the lipid droplets (green), which contributed to the formation of the interfacial framework to stabilize the emulsions.

3.5. Lipid oxidation of emulsions

Emulsion-based products with unsaturated fatty acids are susceptible to oxidation. The oxidation of soybean oil-in-water emulsions was monitored and expressed as the primary oxidation product and secondary oxidation product during the 14 days of storage.

As shown in Fig. 6a, the PV value of the emulsion stabilized with only GLT was much higher than that of GLT–BLP colloidal complexes after 14 days of storage. With the increase in the BLP–to–GLT mass ratio, the PV value of the emulsion stabilized with GLT–BLP colloidal complexes decreased. Similar results have been reported in previous studies that assessed the anti-oxidative ability of resveratrol and protein complexes in corn-oil emulsions (Wan, Wang, Wang, Yuan, & Yang, 2014).

Lipid oxidation of soybean oil-in-water emulsions was further assessed using the TBARS assay. From Fig. 6b, TBARS showed a rapid increase after 8 days of storage in GLT stabilized emulsions, while the emulsions containing BLPs showed slower and lower increases, indicating that the generation of secondary oxidation products could be effectively retarded. BLPs behaved as effective antioxidants in emulsions because the oil droplets were surrounded by a layer of colloidal complexes, which acted as a coating material to scavenge the oxidant at the interface, preventing lipid oxidant of the corn material (soybean oil). As shown in the above-mentioned assays, the efficiency of colloidal complexes in preventing lipid oxidation improves with the increase in BLP–to–GLT ratios, which might also be associated with the formation of the more concentrated coating layer surrounding the lipid droplet.

It's supposed that both free BLPs in the emulsion and bound BLPs in the colloidal complexes contributed to the retard of lipid oxidation. As determined with vanilla assay in the presence of sulfuric acids, only 2.6% and 2.0% of BLPs were unbound when 0.075 wt% and 0.15 wt% of BLPs were used for emulsion preparation. The amount of free BLPs was too low to effectively retard lipid oxidation. Thus, the bound BLPs in the colloidal complexes played a major role in reduced lipid oxidation. Besides, the colloidal complexes absorbed on the surface of lipid droplets formed a thick shell, which generated strong steric repulsion. The thick shell was able to reduce the exposure of lipid to oxygen, which was another way for colloidal complexes to retard lipid oxidation.

4. Conclusion

In summary, the self-assembled GLT–BLP colloidal complexes were formed mainly by hydrogen forces and were employed as effective emulsifiers used to develop stable O/W emulsions. The preparation process of the colloidal complexes was energy efficient and convenient. Compared with many other synthetic materials, the emulsion here was based on food-grade protein and biocompatible natural resources. The incorporation of BLPs had a significant impact on the particle size and surface charge of the colloidal complexes. The antioxidant GLT–BLP colloidal complexes, distributed at the water–oil interface, served as physical barriers against lipid oxidation under storage. Based on the above results, some hydrophobic active ingredients, such as β-carotene, could be dissolved in the internal phase and then prepared in the

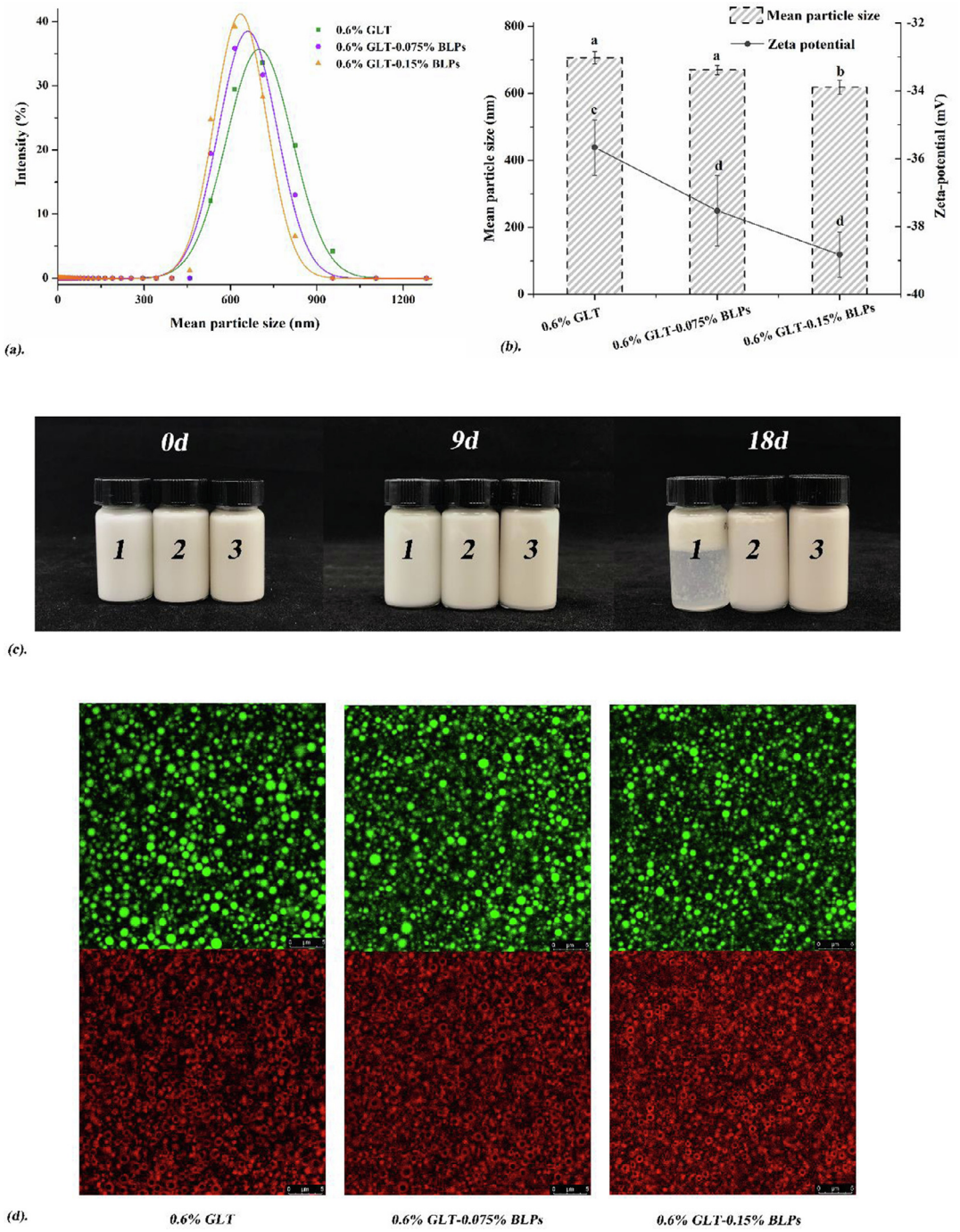

Fig. 5. Size distribution (a), mean particle size, and ζ-potential (b) of oil droplets stabilized by GLT and GLT–BLP colloidal complexes. Photographs of the appearance of emulsions stabilized by 0.6% GLT (1), 0.6% GLT–0.075% BLPs (2), and 0.6% GLT–0.15% BLPs (3) after 9 and 18 days of storage at room temperature (c), and confocal laser scanning microscopy (CLSM) images of emulsions stabilized by GLT and GLT–BLP colloidal complexes (d).

emulsion, forming a colloidal complex membrane around the oil phase, which encapsulates the active ingredients and also enhance the bioavailability of them, providing new opportunities for the use of GLT–BLP–stabilized emulsions in functional food applications.

CRediT authorship contribution statement

Shiguo Chen: Supervision, Writing - review & editing, Funding acquisition. **Xuemin Shen:** Investigation, Writing - original draft. **Wenyang Tao:** Data curation, Validation, Formal analysis. **Guizhu Mao:** Data curation, Validation, Formal analysis. **Wenyan Wu:** Data curation, Validation, Formal analysis. **Shengyi Zhou:** Data curation, Validation, Formal analysis. **Xingqian Ye:** Supervision, Writing - review & editing, Funding acquisition. **Haibo Pan:** Conceptualization, Methodology, Writing - review & editing.

Declaration of Competing Interest

The authors declare that they have no known competing financial interests or personal relationships that could have appeared to influence the work reported in this paper.

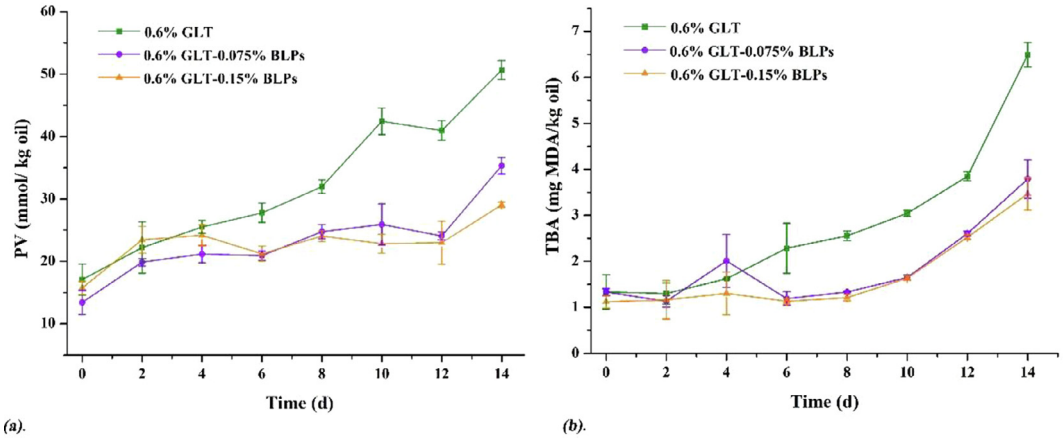

Fig. 6. Lipid hydroperoxides (a) and thiobarbituric acid-reactive substances (TBARS) (b) of GLT–BLP colloidal complexes stabilized emulsions during 14 days of storage.

Acknowledgements

This work was financially supported by Key Research and Development Project of Zhejiang Province, China (2018C02G2011105250) and National Key R&D Program of China (2016YFD0400805104).

References

Berton, C. C., & Schroen, K. (2015). Pickering emulsions for food applications: Background, trends, and challenges. *Annual Review of Food Science and Technology, 6*, 263–297.

Bi, F., Zhang, X., Bai, R., Liu, Y., Liu, J., & Liu, J. (2019). Preparation and characterization of antioxidant and antimicrobial packaging films based on chitosan and proanthocyanidins. *International Journal of Biological Macromolecules, 134*, 11–19.

Chen, Y. C., Yu, S. H., Tsai, G. J., Tang, D. W., Mi, F.-L., & Peng, Y.-P. (2010). Novel technology for the preparation of self-assembled catechin/gelatin nanoparticles and their characterization. *Journal of Agricultural and Food Chemistry, 58*(11), 6728–6734.

Chung, J. E., Tan, S., Gao, S. J., Yongvongsoontorn, N., Kim, S. H., Lee, J. H., ... Ying, J. Y. (2014). Self-assembled micellar nanocomplexes comprising green tea catechin derivatives and protein drugs for cancer therapy. *Nature Nanotechnology, 9*, 907.

Ferraro, V., Madureira, A. R., Fonte, P., Sarmento, B., Gomes, A. M., & Pintado, M. E. (2015). Evaluation of the interactions between rosmarinic acid and bovine milk casein. *RSC Advances, 5*(107), 88529–88538.

Fu, Y., Qiao, L., Cao, Y., Zhou, X., Liu, Y., & Ye, X. (2014). Structural elucidation and antioxidant activities of proanthocyanidins from Chinese bayberry (*Myrica rubra* Sieb. et Zucc.) leaves. *PLoS One, 9*(5), e96162.

Gohtani, S., & Yoshii, H. (2018). 6 – Microstructure, composition, and their relationship with emulsion stability. In S. Devahastin (Ed.). *Food microstructure and its relationship with quality and stability* (pp. 97–122). Woodhead Publishing.

Goodarzi, F., & Zendehboudi, S. (2019). A comprehensive review on emulsions and emulsion stability in chemical and energy industries. *The Canadian Journal of Chemical Engineering, 97*(1), 281–309.

Hammerstone, J. F., Kelm, M. A., Haytowitz, D., Beecher, G., Holden, J., Gebhardt, S., ... Prior, R. L. (2004). Concentrations of proanthocyanidins in common foods and estimations of normal consumption. *The Journal of Nutrition, 134*(3), 613–617.

Huang, H. Y., Wang, M. C., Chen, Z. Y., Chiu, W. Y., Chen, K. H., Lin, I. C., ... Tseng, C. L. (2018). Gelatin-epigallocatechin gallate nanoparticles with hyaluronic acid decoration as eye drops can treat rabbit dry-eye syndrome effectively via inflammatory relief. *International Journal of Nanomedicine, 13*, 7251–7273.

Huang, Y., Li, A., Qiu, C., Teng, Y., & Wang, Y. (2017). Self-assembled colloidal complexes of polyphenol-gelatin and their stabilizing effects on emulsions. *Food & Function, 8*(9), 3145–3154.

Karefyllakis, D., Altunkaya, S., Berton-Carabin, C. C., van der Goot, A. J., & Nikiforidis, C. V. (2017). Physical bonding between sunflower proteins and phenols: Impact on interfacial properties. *Food Hydrocolloids, 73*, 326–334.

Kim, S., Nimni, M. E., Yang, Z., & Han, B. (2005). Chitosan/gelatin–based films cross-linked by proanthocyanidin. *Journal of Biomedical Materials Research Part B: Applied Biomaterials, 75B*(2), 442–450.

Le Bourvellec, C., & Renard, C. M. G. C. (2012). Interactions between polyphenols and macromolecules: quantification methods and mechanisms. *Critical Reviews in Food Science and Nutrition, 52*(3), 213–248.

Li, Z., & Gu, L. (2011). Effects of mass ratio, pH, temperature, and reaction time on fabrication of partially purified pomegranate ellagitannin – gelatin Nanoparticles. *Journal of Agricultural and Food Chemistry, 59*(8), 4225–4231.

Linke, C., & Drusch, S. (2016). Turbidity in oil-in-water-emulsions — Key factors and visual perception. *Food Research International, 89*, 202–210.

Liu, C., Li, M., Yang, J., Xiong, L., & Sun, Q. (2017). Fabrication and characterization of biocompatible hybrid nanoparticles from spontaneous co-assembly of casein/gliadin and proanthocyanidin. *Food Hydrocolloids, 73*, 74–89.

Lobo, L. (2002). Coalescence during emulsification: 3. Effect of gelatin on rupture and coalescence. *Journal of Colloid and Interface Science, 254*(1), 165–174.

Muyonga, J. H., Cole, C. G. B., & Duodu, K. G. (2004). Fourier transform infrared (FTIR) spectroscopic study of acid soluble collagen and gelatin from skins and bones of young and adult Nile perch (Lates niloticus). *Food Chemistry, 86*(3), 325–332.

Naczk, M., & Shahidi, F. (2006). Phenolics in cereals, fruits and vegetables: Occurrence, extraction and analysis. *Journal of Pharmaceutical and Biomedical Analysis, 41*(5), 1523–1542.

Ou, K., & Gu, L. (2014). Absorption and metabolism of proanthocyanidins. *Journal of Functional Foods, 7*, 43–53.

Qiu, C., Huang, Y., Li, A., Ma, D., & Wang, Y. (2018). Fabrication and characterization of oleogel stabilized by gelatin-polyphenol-polysaccharides nanocomplexes. *Journal of Agricultural and Food Chemistry, 66*(50), 13243–13252. https://doi.org/10.1021/acs.jafc.8b02039.

Qiu, C., Zhao, M., Decker, E. A., & McClements, D. J. (2015). Influence of protein type on oxidation and digestibility of fish oil-in-water emulsions: Gliadin, caseinate, and whey protein. *Food Chemistry, 175*, 249–257.

Rao, A., Kim, J., & Thomas, R. R. (2005). Interfacial rheological studies of gelatin – sodium dodecyl sulfate complexes adsorbed at the air – water interface. *Langmuir, 21*(2), 617–621.

Ricci, A., Olejar, K. J., Parpinello, G. P., Kilmartin, P. A., & Versari, A. (2015). Application of fourier transform infrared (FTIR) spectroscopy in the characterization of tannins. *Applied Spectroscopy Reviews, 50*(5), 407–442.

Scott, L. R., & Fernández, A. (2017). Aromatic Interactions.

Smeriglio, A., Barreca, D., Bellocco, E., & Trombetta, D. (2017). Proanthocyanidins and hydrolysable tannins: Occurrence, dietary intake and pharmacological effects. *British Journal of Pharmacology, 174*(11), 1244–1262.

Su, Y. R., Tsai, Y. C., Hsu, C. H., Chao, A. C., Lin, C. W., Tsai, M. L., & Mi, F. L. (2015). Effect of grape seed proanthocyanidin-gelatin colloidal complexes on stability and in vitro digestion of fish oil emulsions. *Journal of Agricultural and Food Chemistry, 63*(46), 10200–10208.

Surh, J., Decker, E., & McClements, D. (2006). Properties and stability of oil-in-water emulsions stabilized by fish gelatin. *Food Hydrocolloids, 20*(5), 596–606.

Tong, L. M., Sasaki, S., McClements, D. J., & Decker, E. A. (2000). Antioxidant activity of whey in a salmon oil emulsion. *Journal of Food Science, 65*(8), 1325–1329.

Wan, Z. L., Wang, J. M., Wang, L. Y., Yuan, Y., & Yang, X. Q. (2014). Complexation of resveratrol with soy protein and its improvement on oxidative stability of corn oil/water emulsions. *Food Chemistry, 161*, 324–331.

Waters, M. L. (2013). Aromatic Interactions. *Accounts of Chemical Research, 46*(4) 873–873.

Zarai, Z., Balti, R., Sila, A., Ali, Y. B., & Gargouri, Y. (2016). Helix aspersa gelatin as an emulsifier and emulsion stabilizer: Functional properties and effects on pancreatic lipolysis. *Food & Function, 7*(1), 326–336.

Zhang, Y., Zhou, X., Tao, W., Li, L., Wei, C., Duan, J., ... Ye, X. (2016). Antioxidant and antiproliferative activities of proanthocyanidins from Chinese bayberry (*Myrica rubra* Sieb. et Zucc.) leaves. *Journal of Functional Foods, 27*, 645–654.

Zhou, F. Z., Yan, L., Yin, S. W., Tang, C. H., & Yang, X. Q. (2018). Development of pickering emulsions stabilized by gliadin/proanthocyanidins hybrid particles (GPHPs) and the fate of lipid oxidation and digestion. *Journal of Agricultural and Food Chemistry, 66*(6), 1461–1471.

Zou, T., Li, Z., Percival, S. S., Bonard, S., & Gu, L. (2012). Fabrication, characterization, and cytotoxicity evaluation of cranberry procyanidins-zein nanoparticles. *Food Hydrocolloids, 27*(2), 293–300.